



Protein coverage on silicon surfaces modified with amino-organic films: A study by AFM and angle-resolved XPS

K. Awsiuk^a, A. Bernasik^b, M. Kitsara^{c,e}, A. Budkowski^{a,*}, J. Rysz^a, J. Haberko^b, P. Petrou^d, K. Beltsios^e, J. Raczowska^a

^a M. Smoluchowski Institute of Physics, Jagiellonian University, Reymonta 4, 30-059 Kraków, Poland

^b Faculty of Physics and Applied Computer Science, AGH-University of Science and Technology, Al. Mickiewicza 30, 30-059 Kraków, Poland

^c Institute of Microelectronics, NCSR "Demokritos", End Patriarchou Gregoriou Str., 15310 Aghia Paraskevi, Greece

^d Institute of Radioisotopes & Radiodiagnostic Products, NCSR "Demokritos", End Patriarchou Gregoriou Str., 15310 Aghia Paraskevi, Greece

^e Materials Science and Engineering Department, University of Ioannina, 45110 Ioannina, Greece

ARTICLE INFO

Article history:

Received 22 January 2010

Received in revised form 21 May 2010

Accepted 22 May 2010

Available online 1 June 2010

Keywords:

Amino-organic bilayers

Gamma globulins

Silanized silicon

Angle-resolved X-ray photoelectron spectroscopy

Atomic force microscopy

Integral geometry analysis

ABSTRACT

An approach to determine structural features, such as surface fractional coverage F and thickness d of protein layers immobilized on silicon substrates coated with amino-organic films is presented. To demonstrate the proposed approach rabbit gamma globulins (RgG) are adsorbed from a $0.66 \mu\text{M}$ solution onto SiO_2 and Si_3N_4 modified with (3-aminopropyl)triethoxysilane (APTES). Atomic force microscopy data are analyzed by applying an integral geometry approach to yield average coverage values for silanized Si_3N_4 and SiO_2 coated with RgG, $F = 0.99 \pm 0.01$ and 0.76 ± 0.08 , respectively. To determine the RgG thickness d from angle-resolved X-ray photoelectron spectroscopy (ARXPS), a model of amino-organic bilayer with non-homogeneous top lamellae is introduced. For an APTES layer thickness of $1.0 \pm 0.1 \text{ nm}$, calculated from independent ARXPS measurements, and for fractional surface RgG coverage determined from AFM analysis, this model yields $d = 1.0 \pm 0.2 \text{ nm}$ for the proteins on both silanized substrates. This value, confirmed by an evaluation ($1.0 \pm 0.2 \text{ nm}$) from integral geometry analysis of AFM images, is lower than the RgG thickness expected for monomolecular film ($\sim 4 \text{ nm}$). Structures visible in phase contrast AFM micrographs support the suggested sparse molecular packing in the studied RgG layers. XPS data, compared for bulk and adsorbed RgG, suggest preferential localization of oxygen- and nitrogen-containing carbon groups at silanized silicon substrates. These results demonstrate the potential of the developed AFM/ARXPS approach as a method for the evaluation of surface-protein coverage homogeneity and estimation of adsorbed proteins conformation on silane-modified silicon substrates used in bioanalytical applications.

© 2010 Elsevier B.V. All rights reserved.

1. Introduction

Every surface's contact with a biological environment is governed by the properties of adsorbed proteins. These properties are extremely important for bioengineering, biocompatibility and biotechnology applications. For biosensors, the proteins immobilized on a surface must also preserve their specific reactivity towards their counterpart molecules. Therefore the quality of biosensing device is especially dependent on the structural features, such as amount (thickness) and arrangement (homogeneity or fractional coverage) of the proteins on surface.

Structural properties of adsorbed proteins, such as commonly studied mammal immunoglobulins [1–8], are usually probed

locally with atomic force microscopy AFM or examined globally with other techniques. Various approaches have been developed to extract structural information from experiments performed with proteins with different surface organization. For *individual proteins* or their *separate aggregates* covering sparsely flat reference *inorganic surfaces*, AFM height histograms are analyzed to yield average height of protein molecules [2–4,9,10]. In addition, threshold analysis of AFM micrographs visualizes (with binary black-and-white images) the shape of surface patterns indicating protein orientation [2] or conformation [11]. We have recently demonstrated [12–14] that for *non-homogeneous layers* integral geometry approach [15–17], which includes both histogram and threshold methods, can fully characterize the vertical extent of organic surface patterns [12] and the morphology (i.e. fractional coverage, shape and connectivity) of protein patches [13,14]. In turn, the thickness of *continuous protein layers* is usually evaluated with global surface anal-

* Corresponding author. Tel.: +48 12 66 35 550; fax: +48 12 63 37 086.

E-mail address: ufbudkow@cyf-kr.edu.pl (A. Budkowski).

ysis techniques such as ellipsometry [7] or surface plasmon resonance [1]. Direct thickness measurements, based on AFM analysis of scratched surface regions [18–21], have recently verified [18] angle-resolved X-ray photoelectron spectroscopy (ARXPS) as a technique suitable for the nanometer thickness determination of homogeneous organic layers covering inorganic surfaces.

In contrast to the simple model systems using inorganic hard surfaces as a substrate, proteins deposited on biosensing devices are usually immobilized on surfaces previously modified with soft amino-organic films, which makes some existing thickness determining methods, such as AFM tip-scratch [18,19,21] or ARXPS [18], hardly applicable. In addition, although homogeneous protein layers are commonly required, surface inspection approach should also provide information about non-uniform protein coverage. Such an approach combining AFM and ARXPS is presented in this study. Within this approach the integral geometry analysis [12–14] of AFM micrographs and a bilayer extension of existing ARXPS models [18,22] are applied to characterize the uniformity of surface's protein coverage. AFM analysis provides not only the fractional surface coverage, necessary to determine with ARXPS the protein thickness, but also confirms the obtained thickness value.

The proposed method enables a complete structural characterization of protein layers immobilized on surfaces pre-modified with soft amino-organic films. The method gains information from the association of surface morphology measurements (e.g. coverage), averaged from AFM data probed locally at various spots, with thickness evaluation, based on global spectroscopic examination. While AFM-based morphological measurements [11,13,14] and spectroscopic thickness evaluations [7] were analyzed previously for non-uniform protein layers with void volume fractions, they have not been combined so far in one approach. Finally, ARXPS-based spectroscopic thickness determination, demonstrated earlier for polymer films [18], is now extended to protein layers. In addition to these unique features, the new AFM/ARXPS approach confirms other recently reported properties, such as identification of surface domains based on image analysis of various AFM modes [23], or preferential orientation of specific functional carbon groups yielded by ARXPS [24].

2. Materials and methods

2.1. Surface modification and protein adsorption

The silicon substrates used are silicon wafers purchased from Montco Silicon Technologies, Inc. (Spring City, PA, USA) on which either a thermally grown silicon dioxide layer of 1000 nm thickness (SiO_2 surfaces) or an additional silicon nitride layer of 150 nm thickness (Si_3N_4 surfaces) were deposited by low pressure chemical vapor deposition. Cleaning and hydrophilization of the silicon substrates included immersion in 1:1 (v/v) HCl/ CH_3OH solution for 20 min, washing with distilled water and drying with nitrogen flux. The hydrophilized surfaces were then modified with (3-aminopropyl)triethoxysilane (APTES; Sigma Chemical Co., St. Louis, MO, USA), through immersion in a 2% (v/v) aqueous APTES solution for a 2 min, gentle washing with distilled water, drying with nitrogen, and curing at 120 °C for 20 min. To form protein layers on the silanized silicon substrates, the surfaces were incubated with a 100 $\mu\text{g}/\text{mL}$ (0.66 μM) solution of rabbit gamma globulins (RgG; Sigma Chemical Co., St. Louis, MO, USA) in 50 mM carbonate buffer, pH 9.2, for 1 h at room temperature. Then the samples were washed with 50 mM phosphate buffer, pH 7.4, and distilled water and dried with nitrogen.

2.2. Microscopic (AFM) and spectroscopic (ARXPS) surface characterization

Topography and phase contrast images of the silicon (SiO_2 and Si_3N_4) substrates, prior and after each surface modification step of silanization and protein adsorption, were collected in air at room temperature with atomic force microscopes (The Academia System and MultiView 1000, Nanonics Imaging Ltd., Israel) working in non-contact mode. AFM micrographs were analyzed with integral geometry approach [15–17] with the software developed in our laboratory using the procedures described in details in our earlier papers [12–14]. Average values of fractional surface coverage F with the proteins were obtained from the analysis of several AFM images recorded at various surface spots. Error bars for coverage F and all other quantities, except APTES (D) and RgG (d) thickness, indicate standard deviation of each sample mean value. Error bars for D and d are obtained by the least-square fitting program.

Angle-resolved XPS analysis was performed in a VSW Manchester spectrometer with Al $K\alpha$ radiation (1486.6 eV, 200 W) for the photoelectron take-off angle Θ equal to 0°, 60° and 70°. Operating pressure in the analytical chamber was less than 5×10^{-8} mbar. XPS peaks were charge referenced to the neutral (C–C) carbon C1s peak at 284.6 eV. Spectrum backgrounds were subtracted using the Shirley method.

3. Results and discussion

3.1. Approach to determine protein/amino-organic film/silicon structure

An approach to determine the structure of protein layers immobilized on silicon surfaces coated with amino-organic films is the main result of this study. This method is based on a novel model to analyze ARXPS data (introduced in Section 3.1.1), demonstrated for RgG molecules (Section 3.1.4) adsorbed to SiO_2 and Si_3N_4 surfaces modified with APTES (Section 3.1.3). The fraction of surface area covered by proteins, which constitutes an important parameter of the ARXPS model, is determined from the integral geometry analysis of topography AFM micrographs (Section 3.1.2).

3.1.1. ARXPS model to analyze amino-organic bilayers

To determine with XPS the atomic concentration C_i of every element (ignoring H atoms), corresponding to the photoelectron line with intensity I_i , the following equation is used [18,22,25]:

$$C_i = \frac{I_i / (\sigma_i \lambda_i)}{\sum_j^N I_j / (\sigma_j \lambda_j)} := \frac{X_i}{\sum_j^N X_j} \quad (1)$$

where N includes all elements present in the sample. Essential role in photoelectron spectroscopy, and in Eq. (1), plays the normalized photoelectron intensity $X_i = I_i / S_i$, obtained using sensitivity factors $S_i = \sigma_i \lambda_i$ specified by photoionization cross-sections σ_i [26] and attenuation lengths λ_i [25].

The situation of protein layer covering a continuous amino-organic film on top of silicon substrate can be precisely described. Its structure, depicted schematically in Fig. 1, is characterized by the thickness D of the bottom amino-organic film, as well as by the thickness d and surface fractional coverage F of the protein top layer. Typical thicknesses expected for a monomolecular amino-organic brush formed by silanes ($D(\text{APTES}) \sim 0.9$ nm [27]) and a monomolecular protein layer ($d(\text{RgG}) \sim 4$ nm [7]) sum up to a value below photoelectron sampling depth 3λ (e.g. $3\lambda = 8.7$ nm for 95% detection of C1s line, excited by Al $K\alpha$ radiation [25]). In addition, the sampling vertical depth $3\lambda \cos \Theta$ can be varied by photoelectron take-off angle Θ (Fig. 1) and reduced even to one-half ($\Theta = 60^\circ$) and around one-third ($\Theta = 70^\circ$) of its 0° value. Therefore angle-resolved

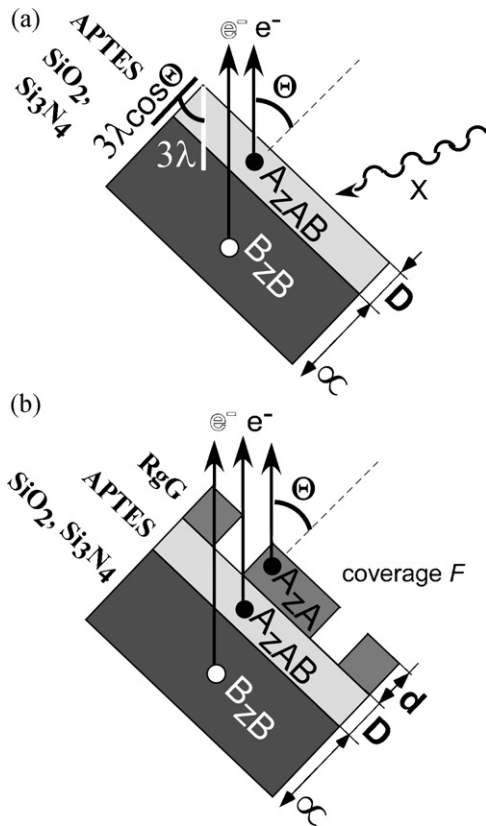


Fig. 1. Model introduced to analyze angle-resolved XPS data. Schematic sectional views of the substrate (SiO_2 , Si_3N_4) coated with amino-organic film of thickness D (APTES brush) (a), and covered additionally with the second (protein) layer, characterized by thickness d and surface fractional coverage F (b). Characteristic photoelectrons are emitted by the element B (here Si), characteristic for the substrate (with molar fraction Z_B), and the element A (here C or amine N), unique for both the amino-organic film (with molar fraction Z_{AB}) and protein layer (Z_A).

X-ray photoelectron spectroscopy ARXPS, using the photoelectrons emitted from both the substrate and the bilayer, is a method sensitive to such structure.

Normalized photoelectron intensity characteristic for the substrate (B, here Si2p peak) and bilayer (A, here C1s or amine N1s line) can be written (see Fig. 1b) as:

$$X_B(\Theta) = \frac{\text{const}}{\lambda_B} \left[(1-F) \int_D^\infty Z_B \exp\left(-\frac{x}{\lambda_B \cos \Theta}\right) dx + F \int_{D+d}^\infty Z_B \exp\left(-\frac{x}{\lambda_B \cos \Theta}\right) dx \right] \quad (2)$$

$$X_A(\Theta) = \frac{\text{const}}{\lambda_A} \left[(1-F) \int_0^D Z_{AB} \exp\left(-\frac{x}{\lambda_A \cos \Theta}\right) dx + F \left(\int_0^d Z_A \exp\left(-\frac{x}{\lambda_A \cos \Theta}\right) dx + \int_d^{D+d} Z_{AB} \exp\left(-\frac{x}{\lambda_A \cos \Theta}\right) dx \right) \right] \quad (3)$$

where in addition to structural parameters (d , D , and F) the stoichiometric molar fractions of the element B (here Si), characteristic for the substrate (Z_B), and the element A (here C or amine N), unique for both the bottom amino-organic film (Z_{AB}) and protein layer (Z_A), are specified.

Taking the ratio of the normalized intensities from bilayer and substrate lines results in

$$\frac{X_A(\Theta)/Z_A}{X_B(\Theta)/Z_B} = \frac{F [1 - \exp(-(d \sec \Theta)/\lambda_A)] + (Z_{AB}/Z_A) [1 - \exp(-(D \sec \Theta)/\lambda_A)] [1 - F + F \exp(-(d \sec \Theta)/\lambda_A)]}{\exp(-(D \sec \Theta)/\lambda_B) [1 - F + F \exp(-(d \sec \Theta)/\lambda_B)]} \quad (4)$$

The structural features of amino-organic (protein/APTES brush) bilayer can be determined with Eq. (4) using ARXPS data. To reduce the number of fitting structural parameters, all the parameters other than protein thickness d are determined independently: the surface fractional coverage F of the top layer is obtained from AFM

analysis and the thickness D of the bottom amino-organic film (APTES brush) from separate ARXPS measurements.

Eq. (4) can be rewritten (for zeroed F value) to obtain the formula which can be used to evaluate the thickness D of singular amino-organic film covering silicon substrate (see Fig. 1a) [18]:

$$\frac{X_A(\Theta)/Z_{AB}}{X_B(\Theta)/Z_B} = \frac{1 - \exp(-(D \sec \Theta)/\lambda_A)}{\exp(-(D \sec \Theta)/\lambda_B)} \quad (5)$$

In practice, the attenuation lengths of the used photoelectrons are comparable ($\lambda_A \approx \lambda_B \approx \lambda$) resulting in a very simple expression for rearranged ratio of photoelectron intensities [18,22]:

$$\ln \left(\frac{X_A(\Theta)/Z_{AB}}{X_B(\Theta)/Z_B} + 1 \right) \approx \frac{D \sec \Theta}{\lambda} \quad (6)$$

This is why the ARXPS data, although rigorously fitted with different λ_i values, are often presented as the sec Θ -dependent plots of the photoelectron intensity ratio according to Eq. (6). In addition, theoretical lines fitting the data in such plots must always start at the origin of coordinate axes, therefore limiting the number of independent data points required.

The stoichiometric molar fractions Z_i of the elements emitting photoelectrons are usually given by the molecular formulas of analyzed compounds [18]. For more complex substances, such as proteins, the Z_A values can be determined with Eq. (1) as atomic concentrations C_i from XPS measurements of the bulk samples. In turn, the fractions Z_{AB} and Z_B , corresponding to the (bottom) amino-organic layer and the substrate, can be evaluated from the ARXPS measurements of the modified substrates (Fig. 1a):

$$Z_{AB} \approx \frac{C_{AB}(\Theta)}{\sum_i^{N_A} C_{A_i}(\Theta)} \quad \text{and} \quad Z_B \approx \frac{C_B(\Theta)}{\sum_i^{N_B} C_{B_i}(\Theta)} \quad (7)$$

where N_A and N_B include all elements present in the layer and in the substrate, respectively. Eqs. (7) are strictly valid when the attenuation lengths of these elements are not too different. In addition, the values Z_{AB} and Z_B obtained from Eqs. (7) are meaningful only when they do not depend on the photoelectron take-off angle Θ : then the inner structure effects of the substrate and the film are negligible. The calculations made with Eqs. (7) are discussed in Section 3.1.3.

3.1.2. Protein fractional coverage from topographic AFM data

To match with the ARXPS model of Fig. 1b, the topography of AFM micrographs should be transformed into representative

black-and-white (binary) images, composed only of two types of surface regions: elevated, i.e. covered by protein layer (white) and depressed, i.e. holes in protein coverage (black). The micrographs represent arrays of pixels set to various levels, proportional to local height values. Each pixel can be reset to either

white or black depending on whether its level value is higher or lower than threshold variable q . The procedures to determine this specific threshold value q , necessary to generate the representative binary images, have been determined within the integral geometry approach [12,14,28]: For bimodal pixel distribution, the

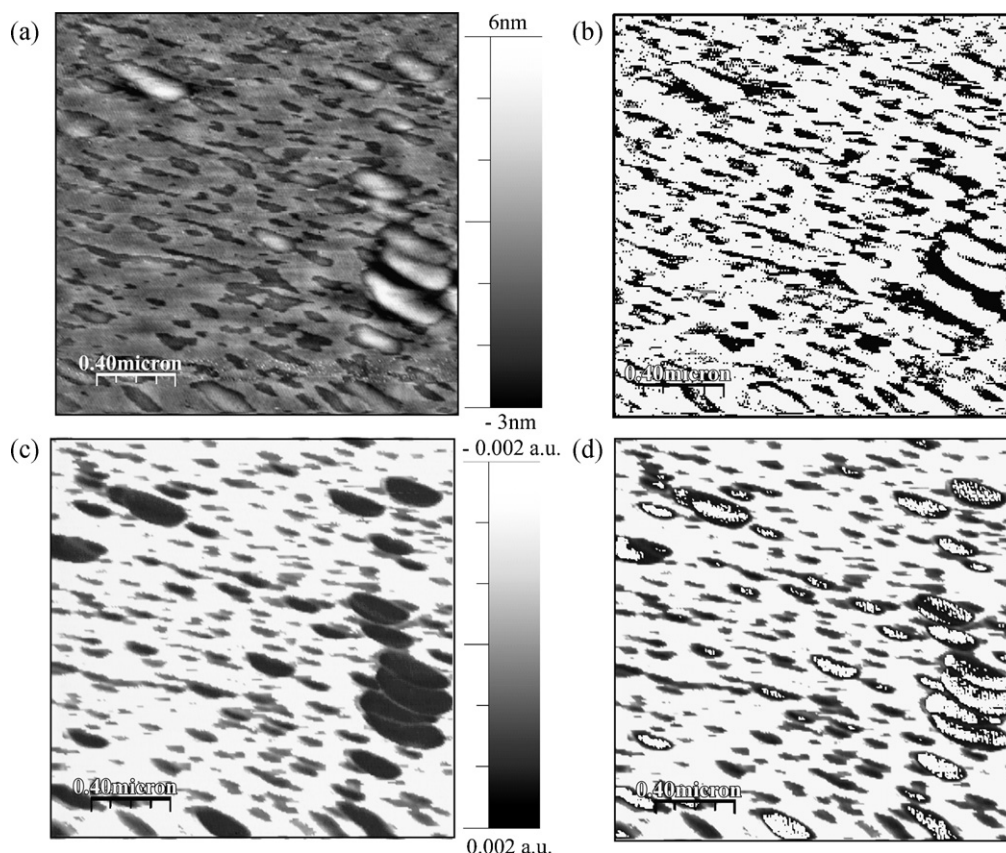


Fig. 2. AFM images and their maps. Topography (a) and phase contrast (c) AFM micrographs, recorded for RgG molecules adsorbed to APTES-coated SiO_2 , and analyzed with integral geometry approach (see Fig. 3) to yield representative binary map of elevated (white) and depressed (black) regions (b) and to mark regions with high phase signal (white) on the phase contrast image (d). Please note the overall correspondence between (b) and (d). Analysis of several black-and-white images (b) yields average fractional surface coverage with elevated regions, $\langle F \rangle = 0.76 \pm 0.08$.

threshold value $q = (H_1 + H_2)/2$ is set by dominant height levels H_1 and H_2 [12]. On the other hand, for monomodal pixel distribution, characterized by its mean H_1 and full-width at half maximum $FWHM$, the specific q value equals to $H_1 \pm 1.69FWHM$ for hole- or island-dominated morphologies, respectively [12]. The representative black-and-white images, generated from AFM micrographs, are fully characterized by the morphological (Minkowski) measures of the white regions [15,16,17], including fractional surface coverage F .

An exemplary topographic micrograph (Fig. 2a) recorded with AFM for RgG proteins adsorbed to silanized SiO_2 surface indicates non-uniform protein coverage. Pixel height distribution of this micrograph, presented in Fig. 3a, is clearly bimodal, thus the dominant heights H_1 and H_2 specify the threshold q value used to compute [12] the representative binary map (Fig. 2b) of high and low surface regions, separated by the height distance $(H_2 - H_1)$. Analysis of representative binary images corresponding to several topography AFM micrographs provides the average fractional coverage with proteins $\langle F \rangle = 0.76 \pm 0.08$, which is required by the ARXPS model. In addition, the averaged height distance $\langle (H_2 - H_1) \rangle$ specifies the averaged protein layer thickness $\langle d \rangle = 1.0 \pm 0.2$ nm, which is further compared with the d value determined from ARXPS results.

In turn, topographic AFM images (Fig. 4a) obtained for RgG molecules adsorbed to silanized Si_3N_4 substrate show uniform protein coverage. As it is shown in Fig. 5a, the corresponding pixel height distributions are monomodal and symmetric. The surface morphology is characterized by singular plateau H_1 with some height fluctuations. Those larger than $1.69FWHM$ (i.e. triple the

width w_F of hyperbolic tangent of integrated pixel distribution $F(q)$ [12]) form singular holes or singular islands – noticeable in AFM images and clearly visible in the computed representative binary black-and-white maps (Fig. 4b and c, respectively). The fractional coverage with proteins F , necessary for the ARXPS model, cannot be lower than that calculated for the elevated regions in the binary maps with singular holes present. Its averaged value, obtained for several AFM micrographs analyzed, is $\langle F \rangle = 0.99 \pm 0.01$.

3.1.3. Amino-organic film thickness from ARXPS measurements

Photoelectron spectroscopy analysis of the APTES films on SiO_2 and Si_3N_4 surfaces is a preliminary step to characterize protein layers. APTES attachment to silicon surfaces is due to APTES hydrolysis followed by surface condensation reaction, and results in a siloxane network terminated with amine groups pointing away from the surface in a brush-like conformation [27,29]. Alternative adsorption mechanism and reversed APTES orientation, driven by protonated amino groups pointing towards (charged) silicon [27], is excluded as no traces of NH_3^+ signal are detected in high resolution XPS spectra of N1s core-level [30,31]. Only the N1s lines characteristic for amine groups (binding energy of 399.7 eV) and for Si_3N_4 (397.2 eV) are observed, the latter present only on nitride substrates.

To comply with the ARXPS model (Fig. 1a), the elements emitting photoelectrons unique for the substrate and the overlayer, respectively, are specified: The silicon (SiO_2 , Si_3N_4) substrate including the silicon–oxygen bonds with the APTES consists of silicon (Si2p core-level, 101.3–102.7 eV), oxygen (O1s, 531 eV) and nitrogen (N1s) in case of Si_3N_4 . In turn, the APTES brush overlayer

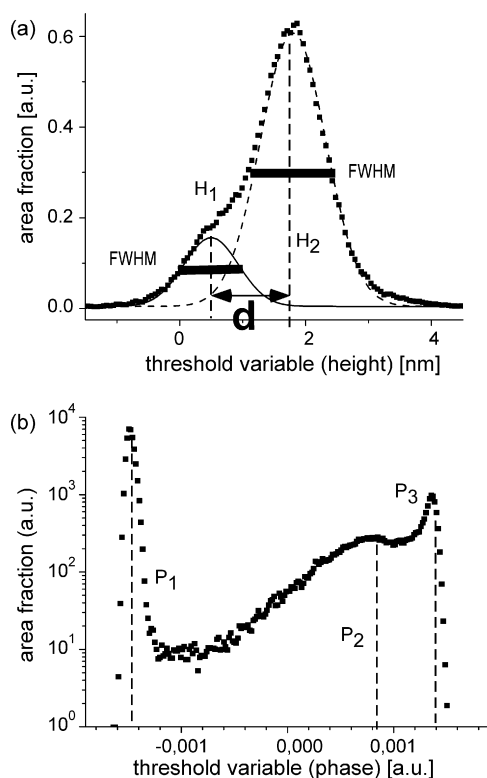


Fig. 3. Analysis of AMF micrographs. Integral geometry analysis of topography (Fig. 2a) and phase contrast (Fig. 2c) images yields bimodal height (a) and trimodal phase signal distribution (b), respectively. Dominant height levels, H_1 and H_2 , specify threshold value $(H_1 + H_2)/2$ to compute representative binary map of high and low regions (see Fig. 2b). Their height distance, $(H_2 - H_1)$, averaged for several micrographs yields $\langle d \rangle = 1.0 \pm 0.2$ nm. Dominant phase signal levels, P_1 , P_2 and P_3 , correspond to white, grey and black regions in Fig. 2c.

is composed of carbon (C1s, 282.1–287.9 eV) and nitrogen (N1s) corresponding to terminal amine groups. For further ARXPS analysis the Si2p peak is taken into account in order to characterize the substrate with respect to stoichiometric Si molar fraction. Z_B values equal to $32.7 \pm 0.6\%$ and $37.5 \pm 0.8\%$ are determined for SiO₂ and Si₃N₄, respectively. The Z_B values are calculated from Eqs. (7) based on ARXPS data, and averaged for Θ angle values between 0° and 70°. These estimations seem reasonable since the first Z_B value accords with nominal SiO₂ stoichiometry (33.3%), while the second one is slightly smaller than the Si₃N₄ stoichiometry (42.8%) due to the presence of oxygen. In addition, the small dispersion of the Z_B value determined for Si₃N₄ indicates that the inner structure of the substrate, e.g. the oxide layer, can be neglected in the ARXPS model. For further analysis, the C1s carbon peak and the N1s line typical for amine groups are taken into account as the most characteristic signals for the silanized Si₃N₄ and SiO₂ substrates, respectively. The corresponding Θ -averaged molar fraction Z_{AB} in the APTES brush calculated from Eqs. (7) is equal to $97.6 \pm 0.7\%$ and $3.2 \pm 0.2\%$ for carbon (on Si₃N₄ substrate) and amine nitrogen (on SiO₂), respectively. This relatively low ratio of nitrogen to carbon content most probably indicates adventitious carbon incorporated in the APTES brush layer [29,32].

The ratios $\ln([X_A(\Theta)/Z_{AB}]/[X_B(\Theta)/Z_B] + 1)$ of normalized intensities of the characteristic photoelectrons for the APTES brush and the silicon substrate are plotted in Fig. 6a versus the take-off angle function $\sec \Theta$. ARXPS data for the silanized SiO₂ and Si₃N₄ are presented as open squares and solid diamonds, respectively. According to Eq. (6), the slopes of the linear regression fitting lines, starting at the origin of axes, would correspond to the thickness D of APTES brush expressed in units of attenuation length λ_i . Both data sets are

fitted rigorously with Eq. (5) (solid lines in Fig. 6a) to yield identical D value of 1.0 ± 0.1 nm, independently of the XPS peak (C1s or amine N1s) used to characterize the APTES overlayer. This D value is in accordance with literature values of 0.9 nm [33] and 1.0 nm [31] determined by ellipsometry. It accords also with the values range of 0.8–1.3 nm reported previously for APTES layers deposited from aqueous solutions [27] and comparable to that (~ 0.9 nm) expected for monomolecular APTES layer [27].

3.1.4. Protein layer thickness from ARXPS measurements

XPS analysis of the solid RgG material yields carbon and amine nitrogen concentration of $C_C = 68.9\%$ and $C_{\text{Namine}} = 11.0\%$, respectively, determined with Eq. (1) from C1s and N1s peak, respectively. The general XPS spectrum of the bulk RgG material indicates also the presence of oxygen ($C_O = 19.7\%$ derived from O1s peak) and sulfur traces ($C_S = 0.3\%$ from S2p peak) but the absence of silicon. Therefore, in the ARXPS analysis the same photoelectrons can be used for the RgG layer as for the underlying APTES brushes, with Si2p peak unique for the silicon substrate, and C1s or amine N1s lines specific for the protein overlayer (and APTES film). The molar fraction Z_A is equal to the bulk RgG value C_C or C_{Namine} , while Z_{AB} and Z_B are identical to those used for silanized silicon substrates.

The ratios $\ln([X_A(\Theta)/Z_A]/[X_B(\Theta)/Z_B] + 1)$ of normalized intensities of the characteristic photoelectrons for the protein/APTES bilayers and the silicon substrate are plotted in Fig. 6b versus the function $\sec \Theta$. The ARXPS data corresponding to RgG molecules immobilized onto silanized SiO₂ and Si₃N₄ substrates are presented as open squares and solid diamonds, respectively. The overlayer/substrate intensity ratio values are distinctly lower for the APTES-modified SiO₂ suggesting lower overall amount of adsorbed proteins as compared to the silanized Si₃N₄. Both data sets are fitted with Eq. (4) (see solid lines in Fig. 6b) to yield the protein layer thickness d values while the other structural parameters, determined independently (fractional coverage with proteins F in Section 3.1.2, APTES brush thickness D in Section 3.1.3), are kept constant. For non-uniform protein coverage on silanized SiO₂ (with $F = 0.76$) the fitting procedure yields a d value equal to 1.0 ± 0.2 nm. The same value is obtained for the RgG proteins covering uniformly ($F = 0.99$) the modified Si₃N₄. This RgG thickness, determined with the extended ARXPS analysis, accords well with the averaged value $\langle d \rangle = 1.0 \pm 0.2$ nm provided by the integral geometry analysis of AFM images, performed for silanized SiO₂ with non-uniform RgG coverage (see Section 3.1.2).

The d value of 1.0 nm, determined here for RgG adsorbed to the silanized silicon from a 0.66 μM solution, is in agreement with the finding of other researchers concerning RgG adsorption to thiolated gold from a solution with comparable concentration of 0.4 μM [7]. In the same study a thickness of uniform RgG layer in the range of 0.5–2.3 nm was determined by ellipsometry for protein concentrations ranging between 0.04 μM and 4 μM [7]. These RgG thickness values are lower than the 4 nm expected for monomolecular layer [3,4,7]. This suggests an inner structure that deviates from a closely packed arrangement of RgG molecules, as it is indeed detected by phase contrast AFM (see Section 3.2.2).

Considering an ARXPS thickness value of 1 nm and a specific volume of 0.745 mL/g [34], an average surface area per RgG molecule of $S_{\text{mol}} = 186 \text{ nm}^2$ is calculated. This can be compared with $S_{\text{mol}} = 97 \text{ nm}^2$ and 46 nm^2 for globulin molecule (ellipsoid with axes 14.5 nm \times 8.5 nm \times 4 nm [8]) with side-on and end-on orientation, respectively. Although for (APTES-like) NH₂ surfaces side-on and end-on antibody alignments have been reported in the literature [35], the higher S value determined in the present study indicates that a side-on protein arrangement [36] is preferred.

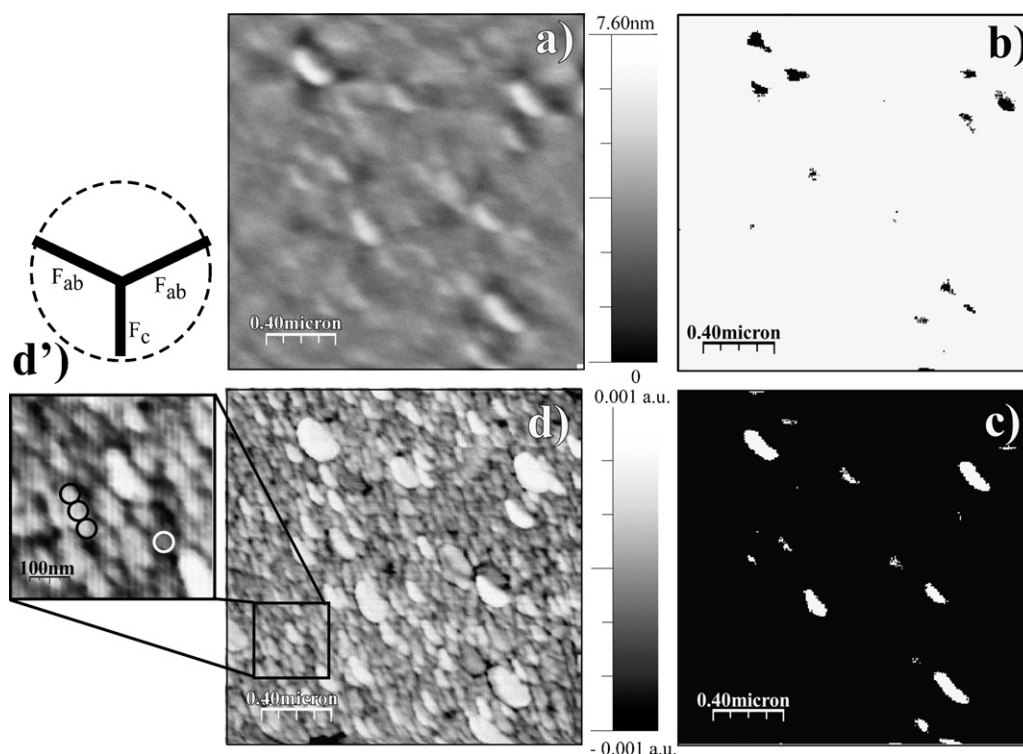


Fig. 4. AFM images and their maps. Topography (a) and phase contrast (d and d') AFM micrographs, recorded for RgG molecules adsorbed to APTES-coated Si_3N_4 , analyzed with integral geometry approach (see Fig. 5) to yield representative binary maps of the regions depressed below (black in b) and elevated above (white in c) the plateau level. Analysis of several black-and-white images (b) yields average surface coverage with elevated regions, $\langle F \rangle = 0.99 \pm 0.01$. Structures revealed in phase contrast images are compared with apparent RgG diameter (circles in d', expected for AFM tip with 20 nm radius of curvature). Please note general correspondence between the regions, which are elevated (white in c) and have high phase signal (white in d).

3.2. Additional features of protein/amino-organic film/silicon structure

Additionally to the basic structural parameters of protein/amino-organic film structure (the parameters D , d , and F in Fig. 1b) determined with the novel approach introduced above, below we present and discuss AFM and XPS results related to other features of the bilayer structures, such as the roughness of their surfaces (Section 3.2.1), the inner structure (Section 3.2.2) and the surface composition (Section 3.2.3) of protein overlayer.

3.2.1. Horizontal versus vertical organization of protein/amino-organic film structure

The vertical organization of the bilayers formed by protein and amino-organic film (see Fig. 1b for the structural model) is characterized by the presence of surfaces separated by 1 nm – the value of D and d thicknesses. These surfaces are not flat and their local heights fluctuate horizontally from one spot to the other. These height variations, specified by root-mean-square RMS roughness R_q , are measured by AFM for each surface prior and after the silanization and protein adsorption steps. RMS roughness characterizes, similarly to $FWHM$, the extent of pixel height distribution ($R_q = FWHM/2 \ln^{0.5}(4)$ for Gaussian). For bare silicon substrates RMS roughness values of $R_q = 0.19 \pm 0.01$ nm for SiO_2 and 0.22 ± 0.05 nm for Si_3N_4 , are determined, which correspond to $FWHM$ of 0.5 nm, indicating smooth and featureless surfaces. After silanization the roughness parameter is still small, with R_q equal to 0.22 ± 0.05 nm and 0.56 ± 0.46 nm for SiO_2 and Si_3N_4 , respectively, reflecting also uniform APTES layers. The corresponding AFM topography and phase contrast images (not provided here) show indeed featureless surfaces similar to those reported previously [37]. Adsorption of RgG increases somewhat the RMS roughness for both silanized surfaces, with R_q equal to 0.55 ± 0.14 nm and 0.75 ± 0.38 nm for

SiO_2 and Si_3N_4 , respectively. The roughness parameters are, within error bars, comparable indicating the larger impact of singular but relatively high protein clusters (~ 7 nm) (see Section 3.2.2) rather than of relatively shallow holes (~ 1 nm) in the non-uniform RgG coverage of silanized SiO_2 .

Schematic sectional views of APTES-modified silicon substrates covered with non-uniform (SiO_2) and uniform (Si_3N_4) protein layer are shown in Fig. 7a and b, respectively. Please note that the sketched boundary lines are taken from AFM cross-sections recorded prior and after each surface modification step of silanization and RgG adsorption. These AFM cross-sections, reflecting surface roughness, are compared with bilayer thicknesses. Vertical and horizontal extent of the sketches in Fig. 7 corresponds to a few and a few hundred nanometers, respectively.

3.2.2. Protein lateral structure from phase contrast AFM data

Phase contrast micrographs, originating from dissipative interactions of AFM tip with the surface, provide information complementary to surface topography. An exemplary phase contrast image, obtained for silanized SiO_2 with non-uniform RgG protein coverage, is presented in Fig. 2c. Three types of surface regions, marked as white, grey and black domains, are clearly visible that correspond to three dominant and consecutive phase signal levels, denoted as P_1 , P_2 and P_3 , respectively, on the corresponding pixel distribution in Fig. 3b. In addition, when the regions with the highest phase signal are also marked in white (for the threshold $q = P_3$), the corresponding modified phase contrast map (Fig. 2d) clearly resembles the binary map of elevated and depressed regions (Fig. 2b). This comparison relates the grey-like P_2 -phase signal domains (Fig. 2d and c) with the depressed regions with no protein coverage (Fig. 2b and a). In turn, the domains with extreme phase signals, P_1 and P_3 , correspond to the regions covered by RgG. The P_3 -like domains (black in Fig. 2c), covering only a few percent of surface

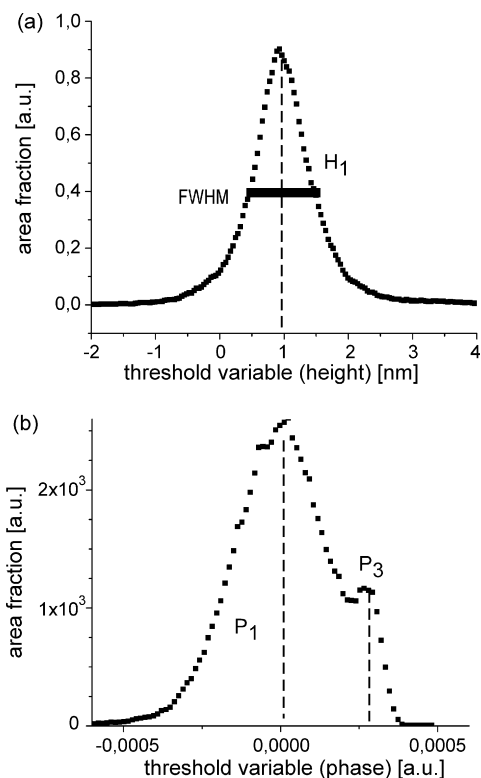


Fig. 5. Analysis of AMF micrographs. Integral geometry analysis of topography (Fig. 4a) and phase contrast (Fig. 4d) images yields monomodal height (a) and bimodal phase signal distribution (b), respectively. Dominant value (H_1) and extent (full-width at half maximum) of height distribution (a) specify threshold values ($H_1 \pm 1.69FWHM$) to compute representative binary maps of the regions elevated above (Fig. 4c) and depressed below (Fig. 4b) the plateau level. Dominant phase signal levels, P_1 and P_3 , correspond to grey and white regions in Fig. 4d.

area, reflect singular but relatively high (~ 7 nm) protein clusters (white in Fig. 2a) that can be formed even on surfaces exposed to low concentration protein solutions [14,38]. The remaining and dominant surface regions (white in Fig. 2c) with the phase signal centered at P_1 are formed by the homogeneous RgG layer with average thickness of 1 nm. To resume, the trimodal phase signal distribution of recorded AFM images (Fig. 3b) reflects surface regions with different friction, adhesion, and/or viscoelasticity. It consists of a very broad peak P_2 , reflecting bare silanized silicon regions, and two more narrow peaks, dominant P_1 and less pronounced P_3 , corresponding to surface regions covered by nanometer protein layer and singular protein clusters, respectively.

A typical phase contrast image, obtained for silanized Si_3N_4 with uniform RgG coverage, is presented in Fig. 4d, while the corresponding pixel distribution of phase signal is shown in Fig. 5b. As bare silanized silicon regions are no longer present, the peak P_2 is now absent resulting in bimodal distribution, again with less pronounced peak P_3 and dominant P_1 . Singular high protein clusters, shown white on representative binary topographic map (Fig. 4c), correspond to P_3 -like phase signal domains (white in Fig. 4d). In addition, the absence of the (previously very broad) peak P_2 makes the dominant contribution of P_1 even more extended (Fig. 5b). This results in an improved contrast of the phase maps. As a consequence the inner structure of nanometer protein layers is resolved (Fig. 4d and d'). The structural features revealed in the phase contrast images are comparable in size with the apparent RgG molecule diameter of 47 nm, marked by circles in Fig. 4d', as expected for an AFM tip with 20 nm radius of curvature and assuming a spherical RgG shape (with 7 nm radius) [3,4]. The inner structure of the uniform protein layer is expected since its determined thickness of

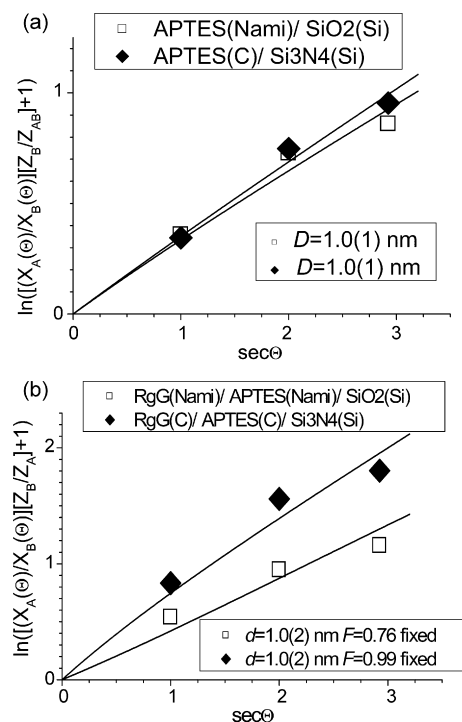


Fig. 6. Analysis of ARXPS data. The overlayer/substrate ratio $\ln([X_A(\Theta)/Z_A(\Theta)]/[X_B(\Theta)/Z_B(\Theta)] + 1)$ plotted versus the take-off angle function $\sec \Theta$ for the substrates (SiO_2 , Si_3N_4) coated with APTES (a) and covered additionally with the RgG layer (b). Regression based on the model in Fig. 1 yields thickness of APTES brush, $D = 1.0 \pm 0.1$ nm, and RgG layer, $d = 1.0 \pm 0.2$ nm, for both substrates with non-uniform (SiO_2) and uniform (Si_3N_4) protein coverage. Assumed F values are taken from integral geometry analysis of AFM micrographs, e.g. Figs. 2b and 4b.

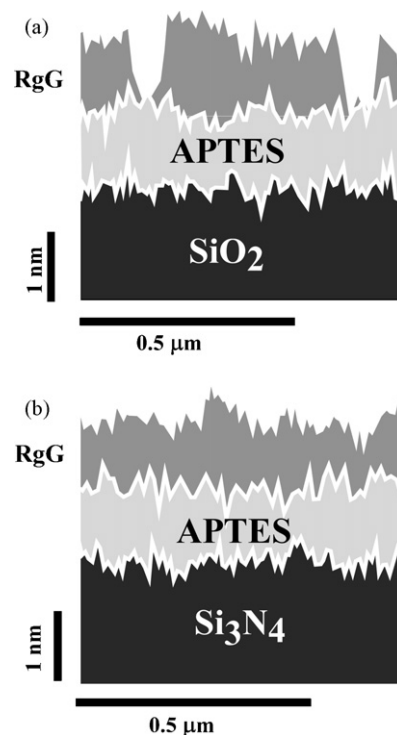


Fig. 7. Schematic sectional views of APTES-coated SiO_2 and Si_3N_4 , with non-uniform (a) and uniform (b) surface coverage with RgG protein layer. Boundary lines are taken from AFM cross-sections recorded prior and after each surface modification step and reflect roughness of silicon substrate, APTES and RgG layer. Vertical and horizontal extent of the figures corresponds to a few and a few hundred nanometers, respectively.

Table 1

Atomic concentration [%] of C, O, Si, amine N, N specific for Si_3N_4 , and S determined for solid RgG and adsorbed RgG layers.

Sample	C 1s	O 1s	Si 2p	N 1s(amine)	N 1s(Si_3N_4)	S 2p
RgG bulk	68.9	19.7	^a	11.0	0.1 ^b	0.3
RgG/APTES/ SiO_2						
$\Theta = 0^\circ$	34.2	42.6	18.6	4.5	0.1 ^b	^a
60°	50.8	29.7	12.6	6.7	0.2 ^b	^a
70°	60.3	23.3	9.4	6.9	0.1 ^b	^a
RgG/APTES/ Si_3N_4						
$\Theta = 0^\circ$	43.0	18.0	18.0	5.1	15.9	^a
60°	59.1	19.7	8.6	8.0	4.6	^a
70°	63.9	18.5	6.9	8.1	2.6	^a

^a Below detection limit.

^b Due to negligible contribution from the group $\text{N}=\text{C}$.

1 nm is below the 4 nm value of monomolecular RgG film (Section 3.1.4).

3.2.3. Chemical composition of adsorbed protein layer versus its bulk phase

ARXPS spectra taken for various photoelectron take-off angles Θ are very sensitive to structural aspects of protein layers. First of all, the atomic concentrations C_i , determined with Eq. (1) and presented in Table 1, differ from those of the bulk sample and vary with Θ , which reflects a finite thickness effect but same composition of RgG layers. For instance, the carbon (C1s) and amine nitrogen (N1s) concentrations determined for the immobilized protein layers are lower than the bulk values but increase with Θ for both modified silicon substrates, when the effective sampling depth is reduced to values more comparable with RgG thickness. In turn, the atomic concentrations characteristic for silanized substrates; silicon (Si2p), oxygen (O1s) for SiO_2 and the nitrogen (N1s) specific for Si_3N_4 ; decrease with take-off angle Θ .

Secondly, it has been recently observed that preferential orientation of specific functional groups with respect to the interface between the adsorbed protein layer and the surface is also reflected in the ARXPS spectra [24]. Therefore, it can be expected that different peaks contributing to the same core-level that correspond to the same element in various functional groups, can be different for the bulk sample and a thin protein layer measured as a function of Θ . This is indeed observed for the C1s core-level spectra of RgG protein in the form of powder and a layer adsorbed to silanized silicon substrate (Fig. 8). The C1s envelope can be resolved into four contributions (Fig. 8a) referred to neutral carbon (C–C) at 284.6 eV and three peaks with modified electron environment positioned at 282.1 eV (C–Si), 286.0 eV (C–O, C–N) and 287.9 eV (C=O, NC=O). It is observed that the fractional contribution of neutral carbon increases from bulk RgG (62.6%) to RgG adsorbed at modified SiO_2 (66.9%) and Si_3N_4 (70.3%), both measured at $\Theta = 0^\circ$. This is accompanied by a reduction of the contribution due to oxygen- and nitrogen-containing carbon groups from 37.4% for bulk RgG to 30.5% and 27.6% for RgG on silanized SiO_2 and Si_3N_4 , respectively. In addition, a distinct decrease of the contribution from the groups with O and N to the C1s envelope is manifested for the proteins adsorbed to modified SiO_2 , when the take-off angle Θ is increased and the effective sampling depth reduced (Fig. 8b). Both observations imply that the O- and N-containing carbon groups are located closer to the protein/silanized silicon interface, suggesting that these groups are important for the protein adsorption process. Similar conclusion has been drawn recently for the adsorption of concanavalin A to a polymer surface [24].

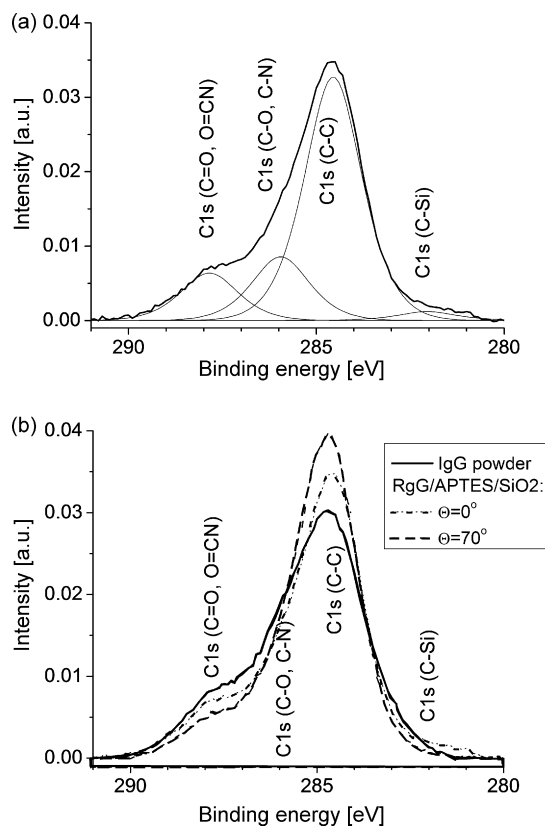


Fig. 8. XPS data compared for powder and adsorbed RgG. (a) Contributions to the C1s core-level spectrum of RgG layer on silanized SiO_2 . (b) C1s spectra of the bulk RgG (solid line) and the RgG layer adsorbed to SiO_2 coated with APTES (dotted-dashed and dashed line for the photoelectron take-off angle of 0° and 70° , respectively), suggesting preferential localization of O- and N-containing carbon group at the protein/silanized silicon interface.

4. Conclusions

We describe a new method for the structural determination of uniform and non-uniform protein layers immobilized onto silicon surfaces coated with soft amino-organic films. Such structures are examined with angle-resolved XPS and AFM by applying a novel ARXPS model of amino-organic bilayer (Section 3.1.1) in combination with an integral geometry approach (Section 3.1.2) extended [13,14] to analyze micrographs of adsorbed proteins. Identical protein layer thickness obtained with ARXPS for uniform (silanized Si_3N_4) and non-uniform (silanized SiO_2) coverage accords also with the evaluation from AFM analysis of the latter system (Section 3.1.4). This verifies the proposed structure determination method. The integral geometry approach to AFM micrographs can be used not only to determine the surface fractional coverage by the proteins but also to relate various domains visible in topographic and phase contrast maps (Section 3.2.2). This allows for a more complete interpretation of the data obtained for the same surface regions with various AFM modes. In addition, phase contrast AFM micrographs reveal an inner structure of protein layers, as it is expected from the fact that the determined protein thickness is below that of monomolecular film. Detailed analysis of core-level XPS and ARXPS spectra reveals preferential orientation of specific functional carbon groups with respect to the interface between the adsorbed protein layer and the substrate (Section 3.2.3), confirming recent protein conformation results for a different protein/substrate system [24].

Acknowledgements

This work was supported by the EU funded project “PYTHIA” (FP7-ICT2-224030). The research was partly carried out with the equipment purchased thanks to the financial support of the European Regional Development Fund in the framework of the Polish Innovation Economy Operational Program (contract No. POIG.02.01.00-12-023/08).

References

- [1] C. Zhou, J.-M. Friedt, A. Angelova, K.-H. Choi, W. Laureyn, F. Frederix, L.A. Francis, A. Campitelli, Y. Engelborghs, G. Borghs, *Langmuir* 20 (2004) 5870, references therein.
- [2] M. Bergkvist, J. Carlsson, T. Karlsson, S. Oscarsson, *J. Colloid Interface Sci.* 206 (1998) 475.
- [3] O. Ouerghi, A. Touhami, A. Othmane, H. Ben Ouada, C. Martelet, C. Fretigny, N. Jaffrezic-Renault, *Biomol. Eng.* 19 (2002) 183.
- [4] O. Ouerghi, A. Touhami, A. Othmane, H. Ben Ouada, C. Martelet, C. Fretigny, N. Jaffrezic-Renault, *Sens. Actuators B* 84 (2002) 167.
- [5] M. Collaud Coen, R. Lehmann, P. Groening, M. Biemann, C. Galli, L. Schlapbach, *J. Colloid Interface Sci.* 233 (2001) 180.
- [6] C. Galli, M. Collaud Coen, R. Hauert, V.L. Katanaev, P. Groening, L. Schlapbach, *Colloids Surf. B* 26 (2002) 255.
- [7] Y. Min Bae, B.-K. Oh, W. Lee, W. Hong Lee, J.-W. Choi, *Biosens. Bioelectron.* 21 (2005) 103.
- [8] K.-B. Lee, S.-J. Park, C.A. Mirkin, J.C. Smith, M. Mrksich, *Science* 295 (2002) 1702.
- [9] H. Agheli, J. Malmstroem, E.M. Larsson, M. Textor, D.S. Sutherland, *Nano Lett.* 6 (2006) 1165.
- [10] J.W. Cheung, G.C. Walker, *Langmuir* 24 (2008) 13842.
- [11] M. Bergkvist, J. Carlsson, S. Oscarsson, *J. Biomed. Mater. Res.* 64 A (2003) 349.
- [12] J. Raczowska, J. Rysz, A. Budkowski, J. Lekki, M. Lekka, A. Bernasik, K. Kowalski, P. Czuba, *Macromolecules* 36 (2003) 2419.
- [13] J. Zemła, M. Lekka, J. Wiltowska-Zuber, A. Budkowski, J. Rysz, J. Raczowska, *Langmuir* 24 (2008) 10253.
- [14] J. Zemła, M. Lekka, J. Raczowska, A. Bernasik, J. Rysz, A. Budkowski, *Biomacromolecules* 10 (2009) 2101.
- [15] K.R. Mecke, *Phys. Rev. E* 53 (1996) 4794.
- [16] J. Becker, G. Grün, R. Seemann, H. Mantz, K. Jacobs, K.R. Mecke, R. Blossey, *Nat. Mater.* 2 (2003) 59.
- [17] K. Michielsen, H. de Raedt, *Phys. Rep.* 347 (2001) 461.
- [18] C. Ton-That, A.G. Shard, R.H. Bradley, *Langmuir* 16 (2000) 2281.
- [19] H. Dvir, J. Jopp, M. Gottlieb, *J. Colloid Interface Sci.* 304 (2006) 58.
- [20] M. Tencer, R. Charbonneau, N. Lahoud, P. Berini, *Appl. Surf. Sci.* 253 (2007) 9209.
- [21] F. Anariba, S.H. DuVall, R.L. McCreery, *Anal. Chem.* 75 (2003) 3837.
- [22] C.S. Fadley, *Prog. Surf. Sci.* 16 (1984) 3.
- [23] F. Orsini, M. Santacroce, P. Arosio, M. Castagna, C. Lenardi, G. Poletti, F.V. Sacchi, *Eur. Biophys. J.* 38 (2009) 903.
- [24] J.A. Mielczarski, J. Dong, E. Mielczarski, *J. Phys. Chem. B* 112 (2008) 5228.
- [25] D. Briggs, *Surface Analysis of Polymers by XPS and Static SIMS*, Cambridge University Press, Cambridge, 1998.
- [26] J.H. Scofield, *J. Electron Spectrosc.* 8 (1976) 129.
- [27] J. Kim, P. Seidler, L. Sze Wan, C. Fill, *J. Colloid Interface Sci.* 329 (2009) 114.
- [28] J. Raczowska, A. Bernasik, A. Budkowski, J. Rysz, K. Kowalski, M. Lekka, P. Czuba, *J. Lekki, Thin Solid Films* 476 (2005) 358.
- [29] J.A. Howarter, J.P. Youngblood, *Langmuir* 22 (2006) 11142.
- [30] D. Kowalczyk, S. Slomkowski, M.M. Chehimi, M. Delamar, *Int. J. Adhes. Adhes.* 16 (1996) 227.
- [31] R. Flores-Perez, A. Ivanisevic, *Appl. Surf. Sci.* 253 (2007) 4176.
- [32] E. Strein, D. Alfred, *Thin Solid Films* 517 (2008) 1011.
- [33] W.L. Leong, P.S. Lee, S.G. Mhaisalkar, T.P. Chen, A. Dodabalapur, *Appl. Phys. Lett.* 90 (2007) 042906.
- [34] D. Givol, E. Hurwitz, *Biochem. J.* 115 (1969) 371.
- [35] S. Chen, L. Liu, J. Zhou, S. Jiang, *Langmuir* 19 (2003) 2859.
- [36] Z.-H. Zhang, C.-L. Feng, *Biotechnol. J.* 2 (2007) 743.
- [37] M.P. Deacon, S. McGurk, C.J. Roberts, P.M. Williams, S.J.B. Tendler, M.C. Davies, S.S. Davis, S.E. Harding, *Biochem. J.* 348 (2000) 557.
- [38] M. Rabe, D. Verdes, S. Seeger, *Soft Matter* 5 (2009) 1039.